Received: 3 December 2020 | Revised: 15 May 2021 | Accepted: 19 May 2021

DOI: 10.1002/mus.27330

CLINICAL RESEARCH ARTICLE

MUSCLE&NERVE WILEY

Three-dimensional quantitative muscle ultrasound in a healthy population

Leon de Jong MSc[1] | Anton Nikolaev MSc[1] | Anna Greco MD[2] | Gert Weijers PhD[1] | Chris L. de Korte PhD[1] | Jurgen J. Fütterer MD, PhD[1]

[1]Department of Imaging, Nuclear Medicine and Anatomy, Radboud Institute for Health Sciences, Radboud University Medical Center, Nijmegen, The Netherlands

[2]Department of Neurology, Radboud University Medical Center, Nijmegen, The Netherlands

Correspondence
Leon de Jong, Radboud University Medical Center, P.O. Box 9101, Internal Postal Code 766, 6500 HB Nijmegen, The Netherlands.
Email: leon.dejong@radboudumc.nl

Funding information
H2020 Industrial Leadership, Grant/Award Number: 688188

Abstract

Introduction/Aims: Quantitative muscle ultrasound offers biomarkers that aid in the diagnosis, detection, and follow-up of neuromuscular disorders. At present, quantitative muscle ultrasound methods are 2D and are often operator and device dependent. The aim of this study was to combine an existing device independent method with an automated ultrasound machine and perform 3D quantitative muscle ultrasound, providing new normative data of healthy controls.

Methods: In total, 123 healthy volunteers were included. After physical examination, 3D ultrasound scans of the tibialis anterior muscle were acquired using an automated ultrasound scanner. Image postprocessing was performed to obtain calibrated echo intensity values based on a phantom reference.

Results: Tibialis anterior muscle volumes of 61.2 ± 24.1 mL and 53.7 ± 22.7 mL were scanned in males and females, respectively. Echo intensity correlated with gender**, age**, fat fraction*, histogram kurtosis**, skewness* and standard deviation** (*$P < .05$, **$P < .01$). Outcome measures did not differ significantly for different acquisition presets. The 3D quantitative muscle ultrasound revealed the non-uniformity of echo intensity values over the length of the tibialis anterior muscle.

Discussion: Our method extended 2D measurements and confirmed previous findings. Our method and reported normative data of (potential) biomarkers can be used to study neuromuscular disorders.

KEYWORDS
muscle ultrasound, neuromuscular disorder, normative data, quantitative ultrasound

1 | INTRODUCTION

Quantitative imaging is being investigated to identify biomarkers for neuromuscular disorders. Several studies investigated the use of such metrics, ie, quantitative MRI (QMRI) and quantitative muscle ultrasound (QMUS).[1-4] Both imaging modalities show promising results in

Abbreviations: AGC, automatic gain control; ANOVA, analysis of variance; BIA, bioelectric impedance analysis; BMI, body mass index; DM, myotonic dystrophy; EI, echo intensity; FOV, field of view; FSHD, facioscapulohumeral dystrophy; IBM, inclusion body myositis; LUT, lookup table; MMT, manual muscle testing; MRC, Medical Research Council; MVC, maximum voluntary contraction; QMRI, quantitative MRI; QMUS, quantitative muscle ultrasound; ROI, region of interest; TGC, time gain compensation; US, ultrasound.

having additional value in detection, diagnosis and follow-up.[5-7] However, incorporation into the clinical routine requires methods that are robust while preserving the quality of the outcome.

Current QMUS methods involve 2D samples of muscle tissue and depend on homogeneously affected tissue as only the sampled cross-section is used for analysis. Myopathies, such as myotonic dystrophy (DM), facioscapulohumeral muscle dystrophy (FSHD), and inclusion body myositis (IBM), that progress in a heterogeneous fashion[8-11] may result in incomplete or false negative outcomes. For this reason, an expansion of the imaged muscle area from a single cross-section to the entire muscle volume in 3D would be desirable.

In addition to the potential sampling error, QMUS is limited by the field of view (FOV) defined by the contact area of the transducer and penetration depth. Amongst others, common parameters that affect QMUS outcome are acquisition settings, vendor dependent post-processing, and manual probe handling.[12] Despite the potential shown in research settings, these influences have hindered the adoption of QMUS in clinical practice and require adequate solutions to overcome these limitations. Opportunities lie in standardizing the acquisition protocol and providing an ultrasound (US) machine independent method. The latter has already been proven feasible as reproducible QMUS parameters can be obtained by using two different US devices.[12] Moreover, a postprocessing method based on a calibration step using a phantom reference enables device independent QMUS.[13]

The purpose of this study is to combine this device independent QMUS method with an automated US machine and perform QMUS in 3D, providing new normative data of healthy controls that can be used for future reference.

2 | METHODS

2.1 | Subject inclusion

All measurements were performed at NEMO Science Museum, Amsterdam, during a science festival. In an inclusion period of 7 days, museum visitors were recruited and received all required information for participation from the researchers. All visitors over the age of 18 y with no relevant (prior) history of disease to the lower limb muscles were allowed to participate.

This study was approved by the institutional review board. Written informed consent was collected from all volunteers.

2.2 | Physical examination

The measurement protocol consisted of two main parts that were both performed within a single visit. The first part consisted of a physical examination performed by a physician and included the following assessments: Hand grip strength, manual muscle testing (MMT) graded according to the Medical Research Council (MRC), height, weight, and bioelectric impedance analysis (BIA). Hand grip strength was measured twice for each hand using a dynamometer (KLS Martin Group, Germany). The maximum value for each hand was used for analysis. MMT included the following muscle groups: neck flexors and extensors, bilateral shoulder external rotators, shoulder horizontal adductors and abductors, elbow flexors and extensors, wrist flexors and extensor, hip flexors, hip abductors, knee flexors and extensors, foot dorsiflexors and plantar flexors. A Tanita BC 601 (Tanita corporation, Tokyo, Japan) BIA scale was used for measurements of weight and BIA parameters. Segmental BIA parameters (arms/legs/core) were fat fraction and muscle mass.

2.3 | Scanning procedure

The second part of the measurement protocol was the actual 3D QMUS measurement. A dedicated US setup was built in order to perform controlled isometric contractions of the tibialis anterior muscle (Supporting Informatio Figure SS1). All measurements were performed on the right leg of each subject, and left/right dominance was recorded. Subjects were supine with their knee slightly bent and a pillow supporting the leg. Once the subject was positioned, a line was drawn below the knee at 1/3 of the distance from the patella to the lateral malleolus. This mark was used to center the US probe at the expected largest cross-section of the tibialis anterior muscle. Scans were made with the US probe oriented in the transverse direction. Prior to the US acquisition, the Sauter FL-S force sensor (Sauter GmbH, Balingen) was referenced to zero, after which the maximum voluntary contraction (MVC) force was measured by recording the maximum value of three attempts. Next, the automated US acquisitions were made using an Acuson S2000 with ABVS module (Siemens Healthineers, Erlangen). The ABVS module contains a 15 cm wide linear array US probe that can automatically move in a linear trajectory within the module. US settings were based on manufacturer preset B and C; 4 or 4.5 cm echo depth, a central frequency of 9 or 10 MHz, and two focal points at 1/3 and 2/3 of the depth for presets 'B' or 'C' respectively. These two different presets were used in order to slightly adapt the FOV, placing the fixed focal points within the muscle tissue. To verify that echo intensity (EI) results were independent of the preset used, a two-tailed paired T-test was performed to rule out a systematic difference in outcome parameters based on the preset used. Any optional postprocessing available within the software was switched off and time gain compensation (TGC) buttons were kept in their neutral positions.

In total, up to three acquisitions were made depending on the subject's ability to perform the exercise; at rest, 20% of MVC, and 40% of MVC. A single acquisition in which the probe automatically moves over the leg in a caudo-cranial direction took about 60 s. In order to maintain a stable exerted force at the required level during scanning, the real-time force graph was shown to the subject with reference lines at 20% or 40% MVC depending on the required acquisition (Supporting Information Figure SS1). The subject was allowed to practice a few times until he or she was able to maintain a stable force within small margins (±5%).

2.4 | Quality control

Acquisitions were performed by a member of the research team, either alone or with individuals who were not part of the research team but who received instructions and were supervised on site by a research team member. Instructions covered the correct positioning of the subject, marking the muscle for centering of the probe, application of US gel, positioning of the transducer module, checking for transducer-skin contact, and starting the automated US acquisition.

2.5 | Postprocessing

After acquisition, all processing steps of the DICOM images were performed using custom-built scripts and MATLAB software (MathWorks Inc. version R2017a). An overview of postprocessing steps is show in Supporting Information Figure SS2. The original DICOM input contained volumetric data of 152 × 152 × 40/45 mm in size, depending on the preset used.

2.5.1 | Segmentation

The first step in postprocessing was segmentation of the tibialis anterior muscle. The selected region of interest (ROI) contained all tissue of the tibialis anterior without the surrounding fascia. Segmentation was performed semi-automatically by manually drawing a ROI surface over the tibialis anterior tissue in the transverse image planes at 5%, 20%, 50%, 80%, and 95% of the total length of the scanned volume. For all slices in between the manually segmented slices, ROI volumes were automatically generated by linear interpolation between the manual ROIs. If no ROI was drawn in a manual slice (eg, no tibialis anterior visible due to lack of contact), the interpolation was not performed and consequently all slices in between were discarded. All segments were available in 98%, 96%, and 100% of all subjects in rest, at 20% MVC force, and at 40% MVC force, respectively. For each subject, all scans were segmented separately as the probe was slightly repositioned after each scan. The resulting segmented volumes were stored as binary ROI volumes for further processing.

2.5.2 | EI corrections

The main quantitative parameter of this study was EI. Obtaining the EI and other QMUS parameters required gray level corrections that were calibrated once for each preset used. After this step, the corrections were applied to all scans that were made with the same preset. EI corrections were based on the work of Weijers et al[14] and consisted of three steps; lookup table (LUT) linearization, automatic gain control (AGC), and noise removal. Linearization of the gray values was based on the LUT available in the DICOM image. The specific curves for B and C presets were therefore corrected to represent a log linear curve. Background, gamma, and AGC were determined using QA4US software[15] and a multipurpose multi-tissue CIRS 040 GSE quantitative phantom with a known attenuation coefficient of 0.95 dB/cm/MHz and containing contrast cylinders. After all corrections, the gray level values were expressed in dB. Mean EI values were calculated by averaging the corrected gray level values of all pixels within the ROI.

The transducer used in this study had a lens with significantly degraded parts, causing persistent noise patterns in the B-mode image. Therefore, any transducer specific noise patterns needed to be excluded from further analysis (Supporting Information Figure SS3). After performing all EI corrections, the resulting gray level images represented EI values expressed in dB.

2.5.3 | Additional parameters

After creating ROI volumes and applying the gray level correction of images, secondary QMUS parameters were extracted. The following (histogram) parameters were extracted: SD of EI, muscle area, entropy, attenuation coefficient, kurtosis, and skewness. These values were calculated for each separate slice. Entropy is a measure for image homogeneity or heterogeneity, for lower or higher values, respectively. Histogram kurtosis and skewness reveal how the gray level values are distributed, with high kurtosis indicating the presence of dominant gray level intensities. Skewness indicates where the most frequent gray levels are present, either on the lower intensity values (dark) for positive skewness or the higher intensity values (bright) for negative skewness.

2.6 | Statistical analysis

Statistical analysis was performed using SPSS software (IBM Corp. version 25). Linear regression on EI, depending on age and grouped by gender, was performed. Correlations between all measured parameters and demographics were evaluated. Prior to statistical analysis, the QMUS parameters were divided into muscle sections and were averaged for each section. Three muscle sections were defined: cranial, middle, and caudal. Each section covered an equally sized fraction of scanned muscle length. To investigate whether contraction of the muscle had an influence on the resulting EI, two-tailed paired T-tests ($P < .05$) were performed for the segmental mean EI for all three contraction states; 0%, 20%, and 40% MVC.

3 | RESULTS

In total, 123 subjects were scanned resulting in 122 scans at rest, 119 at 20% of MVC, and 119 at 40% of MVC. In one volunteer only, the scan at 40% of MVC was acquired. Missing data at 20% and 40% of MVC were due to the inability of the subject to maintain a stable force during acquisition. An overview of the physical examination results is shown in Table 1. Subjects were highly heterogeneous with regard to body composition and strength.

TABLE 1 Physical examination results

			Male ($n = 64$)	Female ($n = 59$)
Age (y)			37 ± 13.5	38 ± 18
Height (cm)			181 ± 7	167 ± 7
Weight (kg)			82 ± 13.7	67 ± 16
BMI (kg/m^2)			22.6 ± 3.5	20.1 ± 4.7
BIA	Fat fraction (%)	Arms	15.3 ± 7.3	29.0 ± 10.7
		Core	19.8 ± 7.7	28.1 ± 8.8
		Legs	16.3 ± 7.3	33.9 ± 7.8
	Muscle mass (kg)	Arms	4.1 ± 1.8	2.3 ± 0.5
		Core	34.6 ± 7.6	24.6 ± 4.7
		Legs	11.0 ± 3.8	7.3 ± 1.0
Maximum hand grip strength (pounds)		R	124.6 ± 23.7	91.4 ± 21.0
		L	121.5 ± 21.8	85.9 ± 21.1
TA MVC force (N)			191.0 ± 55.3	96.5 ± 34.1

Note: Values are mean ± SD.
Abbreviations: N, Newtons; TA, tibialis anterior.

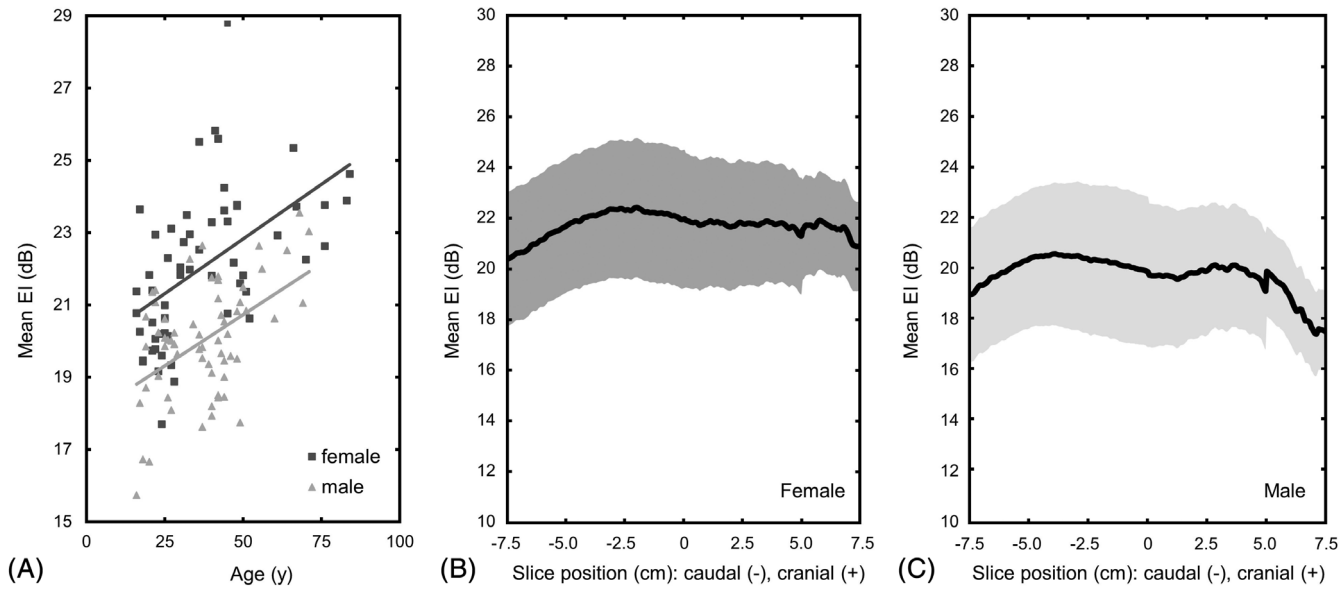

FIGURE 1 A, Bland–Altman plot of mean EI values of the middle muscle segment grouped by gender. Linear regression shows the increasing EI, depending on the subject's age. B,C, confidence plot of mean EI mean ± SD for each measured cross-section at rest. The '0' position indicates the value at 1/3 of the length of the patella to the lateral malleolus

3.1 | Segmentation

Mean ROI volumes of 61.2 and 53.7 mL for males and females, respectively, were found. Supporing Information Table SS1 shows the segmented volumes and fractions of the ROI used after removal of noise areas. The scanned volumes represent the majority of the total muscle volume of the tibialis anterior. The mean scanned muscle volume of 40% MVC scans was on average 17% lower than in scans at rest (two-tailed paired T-test with $P < .001$). After removal of noise areas specific for the transducer used, most (>80%) of the ROI could be used for analysis. Given that the areas with increased noise levels are located at larger echo depths, the proportion of noise increases with muscle thickness (Supporting Information Figure SS3). This explains the slight difference in ROI fraction between male and female subjects, as male subjects generally had thicker muscles.

3.2 | Mean echo intensity values

The Bland–Altman plot (Figure 1(A)) shows the distribution of the mean EI of the middle segment over age, grouped by gender. Linear regression showed an increase of EI by 0.06 dB/y with R^2 0.28 and

0.23 for females and males, respectively. EI levels were significantly higher in women than in men ($p < .001$). In Figure 1B and C, the mean EI is plotted over the length of the tibialis anterior muscle. A similar shape of the EI curve is seen in males and females. In both groups, the mean EI deviates over the length of the muscle with the lowest value measured caudally and gradually increasing to the middle section. The value at position 0 would be the value measured using 2D QMUS.

3.3 | Additional QMUS parameters

The additional parameters calculated were residual attenuation coefficient, entropy, and histogram skewness and kurtosis (Supporting Information Table SS2). The measured attenuation values were within the range of reported values for skeletal muscle; 1.1 ± 0.15 dB/cm/MHz.[16]

3.4 | Correlations

Pearson correlations were calculated and grouped by gender. An overview of the correlation coefficients between age, BMI, and BIA fat fraction in the leg and EI is shown in Table 2. Overall, most of the correlations were of weak to moderate strength, including correlations of multiple histogram parameters with mean EI.

3.4.1 | Muscle contraction

Measurements at different contraction states allowed evaluation of resulting mean EI values; see Table 3. Results showed that, in males, the mean EI value slightly decreased in all muscle segments at increasing MVC states. An exception was seen between rest and 20% MVC states in the middle and the caudal segment. In females, the same trend was seen, with the exception of the middle and caudal segment that did not differ significantly between rest and 20% MVC. In general, there was a tendency that contraction of the muscle lowers the measured EI.

3.4.2 | US settings

In total, 38 subjects were scanned with preset B and 85 with preset C. As a consequence of the calibration we performed, the resulting QMUS outcome should not be different depending on the preset that was used. One-way analysis of variance (ANOVA) revealed no significant differences in the resulting mean EI when grouped by the preset used (mean EI B = 21.1, mean EI C = 20.9 with $P = .80$).

4 | DISCUSSION

The specific curve of resulting EI values over the length of the tibialis anterior muscle indicates the added value of a 3D reference as EI was not uniform throughout the muscle. In the literature, various clinical

TABLE 3 EI levels by muscle stress state

TA segment	Δ MVC (%)	Male Δ EI (dB)	Female Δ EI (dB)
Cranial	0–20	−0.249**	−0.523**
	0–40	−0.575**	−0.645**
Middle	0–20	+ 0.098	−0.159
	0–40	−0.453*	−0.313**
Caudal	0–20	+ 0.260	−0.416
	0–40	−0.796	−0.460*

Note: Two-tailed significance level (*$P < .05$, **$P < .01$).
Abbreviations: dB, decibel; TA, tibialis anterior.

TABLE 2 Correlations between physical examination and quantitative US parameters

Parameter		Age		BMI		BIA legs fat fraction		EI	
		Male	Female	Male	Female	Male	Female	Male	Female
BMI		0.720**	0.240			0.600**	0.720**	0.203	0.436**
BIA Legs	Fat	0.406**	0.457**	0.600**	0.720**			0.286*	0.456**
	Muscle	−0.268*	−0.208	0.381**	0.623**	0.242	0.152	0.075	0.205
Hand strength		−0.619**	−0.142*	0.086	0.038	0.258	−0.307	−0.398**	−0.087
Max force TA		0.027	−0.136	0.369**	0.049	0.128	−0.046	0.090	−0.150
EI		0.484**	0.527**	0.203	0.436**	0.286*	0.456**		
SD		−0.213	−0.142	−0.106	−0.430**	−0.228	−0.326*	−0.422**	−0.452**
Kurtosis		−0.248*	−0.421**	−0.027	−0.134	−0.244	−0.271*	−0.305**	−0.497**
Skewness		−0.418**	−0.440**	−0.226	−0.288*	−0.469**	−0.366**	−0.467*	−0.702**
Entropy		0.176	−0.228	0.011	−0.401**	0.038	−0.313*	−0.005	−0.144
Attenuation		0.046	−0.158	−0.226	−0.539**	−0.312*	−0.476**	−0.222	−0.423**

Note: Values are bivariate Pearson correlation coefficients. Two-tailed significance level (*$P < .05$, **$P < .01$).
Abbreviation: TA, tibialis anterior.

applications for QMUS proved sensitive for pathology based on 2D sampling in patients with neuromuscular diseases.[17,18] EI over the muscle volume and additional parameters presented in this study are an extension of these 2D biomarkers. An advantage of our method is that, for heterogeneously affected tissue, a 2D sampling error can be excluded. Additionally, for monitoring disease progression or the effects of therapy, 3D imaging can be performed non-invasively for entire individual muscle volumes. Studies that investigate neuromuscular disorders with heterogeneous phenotypes can, therefore, benefit most from our data and method. Another potential application that could benefit from our method would be targeted muscle biopsies to reduce biopsy error rate.[19] Using our method, areas of muscle tissue with deviating EI can be detected and used as a biopsy target.

A limitation of our method is that even though most steps in the postprocessing method are automated, segmentation of the muscle tissue still needs to be performed manually. Further automation would overcome this limitation as the whole postprocessing path is then automated and QMUS values can be calculated directly after each acquisition. Various methods for automatic segmentation of muscle tissue in US image are available.[20-22] However, it was not within the scope of this study to implement automatic segmentation at this stage.

The transducer that was used in this study limited the tissue area that could be included in analysis. However, in all cases a minimal coverage of 80% of the total muscle volume could still be used. The use of a transducer with less systematic noise would enable assessment of the full muscle volume.

The tibialis anterior muscle and all other bipennate muscles have a central aponeurosis, forming a hard reflector (bright) that is located in the center of the muscle. In our study, the central aponeurosis was included in the ROI for the segmentation method to be robust and to be consistent with other QMUS findings reported in literature.[23,24] For future research, excluding the central aponeurosis from analysis could be of interest as it would reflect the echogenic properties of the actual muscle tissue.

Deformation of the muscle induced by the transducer cage could alter the angulation of the muscle fibers. These fibers contribute to the resulting US image as they act as US reflectors. The effects of performing isometric contractions (0%, 20%, and 40% of MVC force) were only significant for the cranial segment and in the middle segment in instances of 40% MVC force. As these contractions deform the muscle heavily but only slightly affect the measured EI in extreme cases, we conclude that any deformation due to the pressure of the transducer cage did not influence the QMUS outcome.

In this study, ROI sizes decreased with increasing muscle contraction force. This can be subscribed to the bulging of the muscle causing less skin area to be in contact with the flat US probe. A possible solution would be to use an acoustic coupling medium between the transducer and skin of the target muscle. Using materials that are in existing acoustic gel pads,[25] this approach should be feasible. In this case, the skin surface that needs to be scanned no longer needs to be flat. This would also increase the number of muscles that can be scanned with our method. Thereby extending the field of applications of this method, which could aid the implementation of volumetric muscle scanning in the clinic.

This study was performed under controlled conditions and, therefore, required a dedicated setup. To further develop our method as one that is suitable for implementation in the clinic, the setup for positioning and force measurement could be removed. Both 2D and 3D US acquisitions could be compared to the values reported in this study. We used technical developments in quantitative US and satisfied findings from a recent review by presenting an operator and device independent method for a clinical application.[26] Further optimizations include full automation of postprocessing by implementing automatic segmentation and image postprocessing within the software of US systems. This would only leave a single calibration step with a phantom reference. Therefore, 3D QMUS using automated US offers opportunities to implement 3D QMUS in clinical practice.

5 | CONCLUSIONS

We were able to perform 3D QMUS measurements and confirmed previous findings in the literature for 2D QMUS. Addition of 3D revealed the non-uniformity of EI values over the length of the tibialis anterior muscle. Investigation of correlations between EI and additional quantitative parameters showed that, in addition to age and gender, there were significant correlations with histogram kurtosis, skewness, and SD. Our method and reporting of healthy characteristics can be used to further study neuromuscular disorders.

ACKNOWLEDGMENTS

This study has received funding by the European Union's Horizon 2020 research and innovation programme under grant agreement no. 688188 as part of the MURAB project. This research was part of Science Live, the innovative research programme of NEMO Science Museum that enables scientists to carry out real, publishable, peer-reviewed research using NEMO visitors as volunteers. Science Live is partially funded by KNAW. In addition to funding and providing the facility, both funding sources were not involved in the execution or reporting of this study.

CONFLICT OF INTEREST

None of the authors has any conflict of interest to disclose.

ETHICAL PUBLICATION STATEMENT

We confirm that we have read the Journal's position on issues involved in ethical publication and affirm that this report is consistent with those guidelines.

DATA AVAILABILITY STATEMENT

The data that support the findings of this study are available from the corresponding author upon reasonable request.

REFERENCES

1. Janssen BH, Pillen S, Voet NBM, Heerschap A, van Engelen BGM, van Alfen N. Quantitative muscle ultrasound versus quantitative magnetic

resonance imaging in facioscapulohumeral dystrophy. *Muscle Nerve*. 2014;50:968-975. https://doi.org/10.1002/mus.24247.
2. Arrigoni F, de Luca A, Velardo D, et al. Multiparametric quantitative MRI assessment of thigh muscles in limb-girdle muscular dystrophy 2A and 2B. *Muscle Nerve*. 2018;58:550-558.
3. Martínez-Payá JJ, del Baño-Aledo ME, Ríos-Díaz J, Tembl-Ferrairó JI, Vázquez-Costa JF, Medina-Mirapeix F. Muscular echovariation: a new biomarker in amyotrophic lateral sclerosis. *Ultrasound Med Biol*. 2017;43:1153-1162.
4. Pillen S, Arts IMP, Zwarts MJ. Muscle ultrasound in neuromuscular disorders. *Muscle Nerve*. 2008;37:679-693. https://doi.org/10.1002/mus.21015.
5. Nuñez-Peralta C, Alonso-Pérez J, Llauger J, et al. Follow-up of late-onset Pompe disease patients with muscle magnetic resonance imaging reveals increase in fat replacement in skeletal muscles. *J Cachexia Sarcopenia Muscle*. 2020;11:1032-1046.
6. Jansen M, van Alfen N, van der Sanden MWGN, van Dijk JP, Pillen S, de Groot IJM. Quantitative muscle ultrasound is a promising longitudinal follow-up tool in Duchenne muscular dystrophy. *Neuromusc Disord*. 2012;22:306-317.
7. van Alfen N, Gijsbertse K, de Korte CL. How useful is muscle ultrasound in the diagnostic workup of neuromuscular diseases? *Curr Opinion Neurol*. 2018;31:568-574. https://doi.org/10.1097/WCO.0000000000000589.
8. Turner C, Hilton-Jones D. Myotonic dystrophy: diagnosis, management and new therapies. *Curr Opinion Neurol*. 2014;27:599-606.
9. Wenninger S, Montagnese F, Schoser B. Core clinical phenotypes in myotonic dystrophies. *Front Neurol*. 2018;9:303.
10. Tawil R, Kissel JT, Heatwole C, Pandya S, Gronseth G, Benatar M. Evidence-based guideline summary: evaluation, diagnosis, and management of facioscapulohumeral muscular dystrophy: report of the guideline development, dissemination, and implementation Subcommittee of the American Academy of Neurology and the practice is. *Neurology*. 2015;85:357-364.
11. Tawil R, van der Maarel S, Padberg GW, van Engelen BGM. 171st ENMC international workshop: standards of care and management of facioscapulohumeral muscular dystrophy. *Neuromusc Disord*. 2010;20:471-475.
12. Pillen S, van Dijk JP, Weijers G, Raijmann W, de Korte CL, Zwarts MJ. Quantitative gray-scale analysis in skeletal muscle ultrasound: a comparison study of two ultrasound devices. *Muscle Nerve*. 2009;39:781-786. https://doi.org/10.1002/mus.21285.
13. Zaidman CM, Connolly AM, Malkus EC, Florence JM, Pestronk A. Quantitative ultrasound using backscatter analysis in Duchenne and Becker muscular dystrophy. *Neuromusc Disord*. 2010;20:805-809.
14. Weijers G, Thijssen JM, Starke A, et al. Computer-aided ultrasound diagnosis of hepatic steatosis. *IFMBE Proc*. 2008;22:843-847. https://doi.org/10.1007/978-3-540-89208-3_202.
15. Thijssen JM, Weijers G, de Korte CL. Objective performance testing and quality assurance of medical ultrasound equipment. *Ultrasound Med Biol*. 2007;33:460-471.
16. Nassiri DK, Nicholas D, Hill CR. Attenuation of ultrasound in skeletal muscle. *Ultrasonics*. 1979;17:230-232.
17. Zaidman CM, Malkus EC, Siener C, Florence J, Pestronk A, Al-Lozi M. Qualitative and quantitative skeletal muscle ultrasound in late-onset acid maltase deficiency. *Muscle Nerve*. 2011;44:418-423.
18. Leeuwenberg KE, van Alfen N, Christopher-Stine L, et al. Ultrasound can differentiate inclusion body myositis from disease mimics. *Muscle Nerve*. 2020;61:783-788.
19. Lassche S, Janssen BH, IJzermans T, et al. MRI-guided biopsy as a tool for diagnosis and research of muscle disorders. *J Neuromusc Dis*. 2018;5:315-319.
20. Salvi M, Caresio C, Meiburger KM, De Santi B, Molinari F, Minetto MA. Transverse muscle ultrasound analysis (TRAMA): robust and accurate segmentation of muscle cross-sectional area. *Ultrasound Med Biol*. 2019;45:672-683.
21. Darby J, Hodson-Tole EF, Costen N, Loram ID. Automated regional analysis of B-mode ultrasound images of skeletal muscle movement. *J Appl Physiol*. 2012;112:313-327.
22. Cunningham RJ, Harding PJ, Loram ID. Real-time ultrasound segmentation, analysis and visualisation of deep cervical muscle structure. *IEEE Trans Med Imaging*. 2016;36:653-665.
23. Shahrizaila N, Noto Y, Simon NG, et al. Quantitative muscle ultrasound as a biomarker in Charcot-Marie-tooth neuropathy. *Clin Neurophysiol*. 2017;128:227-232.
24. Mul K, Horlings CGC, Vincenten SCC, Voermans NC, van Engelen BGM, van Alfen N. Quantitative muscle MRI and ultrasound for facioscapulohumeral muscular dystrophy: complementary imaging biomarkers. *J Neurol*. 2018;265:2646-2655.
25. Merrick MA, Mihalyov MR, Roethemeier JL, Cordova ML, Ingersoll CD. A comparison of intramuscular temperatures during ultrasound treatments with coupling gel or gel pads. *J Orthop Sports Phys Ther*. 2002;32:216-220.
26. Oelze ML, Mamou J. Review of quantitative ultrasound: envelope statistics and backscatter coefficient imaging and contributions to diagnostic ultrasound. *IEEE Trans Ultrason Ferroelectr Freq Control*. 2016;63:336-351.

SUPPORTING INFORMATION

Additional supporting information may be found online in the Supporting Information section at the end of this article.

How to cite this article: de Jong L, Nikolaev A, Greco A, Weijers G, de Korte CL, Fütterer JJ. Three-dimensional quantitative muscle ultrasound in a healthy population. *Muscle & Nerve*. 2021;64(2):199–205. https://doi.org/10.1002/mus.27330